Journal of
Materials Chemistry B

Materials for biology and medicine

Accepted Manuscript

This article can be cited before page numbers have been issued, to do this please use: A. Cardellini, C. Caruso, L. Rijns, P. Y. W. Dankers, G. M. M. Pavan and C. Perego, *J. Mater. Chem. B*, 2025, DOI: 10.1039/D5TB01272D.

ROYAL SOCIETY OF CHEMISTRY

rsc.li/materials-b

View Article Online
DOI: 10.1039/D5TB01272D

Journal Name

ARTICLE TYPE

Cite this: DOI: 00.0000/xxxxxxxxxx

Monomer Exchange Dynamics in Ureido-Pyrimidinone Supramolecular Polymers via Molecular Simulations

Annalisa Cardellini,*[a] Cristina Caruso,[b] Laura Rijns,[c,d] Patricia Y.W. Dankers,[c,d,e] Giovanni M. Pavan,[b] and Claudio Perego *[a]

Received Date
Accepted Date

DOI: 00.0000/xxxxxxxxxx

The use of synthetic supramolecular polymers, built by monomers that self-assemble via non-covalent, reversible interactions, is rapidly growing in many fields, including energy, environmental, and bio-engineering applications. Very recently ureido-pyrimidinone (UPy)-based supramolecular polymers have been used to synthetize biocompatible hydrogels aiming to mimic the dynamic environment of extracellular matrices. Tuning the dynamics, stiffness, and bioactivity of UPy-based hydrogels effectively influences cellular behaviour and tissue development. However, a complete understanding of UPy-network dynamics over different length and time scales is still lacking, and even the most advanced experimental approaches are unable to capture the dynamics of monomer exchange with atomistic resolution. Here we present a computational study on UPy supramolecular assemblies in water that uncovers the mechanism of monomer exchange between the UPy-based polymers and their surrounding. Our results, based on atomistic Molecular Dynamics (MD) simulations combined with enhanced sampling and Machine-Learning (ML) techniques show that the fine interplay of solute-solvent interactions is the main engine of supramolecular monomer motion, thereby making UPy polymer ends more dynamic as compared to static UPy polymer backbone. This computational work complements the qualitative experimental evidence on supramolecular dynamics with the mechanism of monomer exchange, revealing the most favorable environment for polymer damage as well as the underlying principle of self-healing.

Living systems possess an intrinsic ability to mitigate a variety of damages, showing self-healing and regenerative properties.[1–3] Inspired by such dynamic features, scientists have been advancing in the synthesis of functional materials with on-demand reversibility and stimuli-responsiveness[4–8]. One common strategy relies on the design of supramolecular materials,[9] i.e., assemblies of non-covalently bound monomers, holding great promise in environmental applications,[10] drug delivery,[11–15] regenerative medicine,[16,17] skin-like stretchable electronics,[18,19] and anticorrosive coatings.[20,21] Examples of monomers forming supramolecular structures include benzene 1,3,5-tricarboxamide (BTA), self-assembling in 1D polymers via core-core stacking and three-fold hydrogen bonding,[22,23] benzotrithiophene building-blocks,[24,25] peptide amphiphiles,[26–28] or metal-coordinated porphyrins.[29–31] In this realm, ureido-pyrimidinone (UPy) molecules have also been largely used by taking advantage of their ability to self-organize in "hierarchical" fibrillar structures in water. Indeed, UPy monomers dimerize by self-complementary quadruple hydrogen bonding in a donor-donor-acceptor-acceptor (DDAA) fashion (Fig. 1a). These planar dimers are the building blocks of fibrillar stacks, which, in turn, can interact to form more complex polymeric polymers.[32–34]

Over the past twenty years, UPy monomers have been functionalized with poly(ethylene glycol) (PEG),[35,36] poly(N-isopropylacrylamide) (PNINAM),[37,38] glycine (Gly) amino acids,[16,39] among others, in order to improve their biocompatibility and tunability.[40] The resulting supramolecular polymers (SPs) have demonstrated intriguing mechanical and dynamic properties in a wide range of multi-component environments, playing a crucial role in the syntheses of biomimetic hydrogels.[41,42] For example, UPy-based SPs have been exploited to mimic the liquid-

* Corresponding Authors: annalisa.cardellini@supsi.ch; cl.perego@supsi.ch
[a] University of Applied Science of Southern Switzerland, SUPSI, via La Santa 1, Lugano, Switzerland; E-mail: annalisa.cardellini@supsi.ch claudio.perego@supsi.ch
[b] Department of Applied Science and Technology, Politecnico di Torino, Corso Duca degli Abruzzi 24, Torino 10129, Italy.
[c] Institute for Complex Molecular Systems, Eindhoven University of Technology, 5600 MB, Eindhoven P.O. Box 513, The Netherlands.
[d] Department of Biomedical Engineering, Eindhoven University of Technology, 5600 MB, Eindhoven P.O. Box 513, The Netherlands.
[e] Department of Chemical Engineering and Chemistry, Eindhoven University of Technology, 5600 MB Eindhoven P.O. Box 513, The Netherlands.
† Supplementary Information available: [details of any supplementary information available should be included here]. See DOI: 00.0000/00000000.

View Article Online
DOI: 10.1039/D5TB01272D

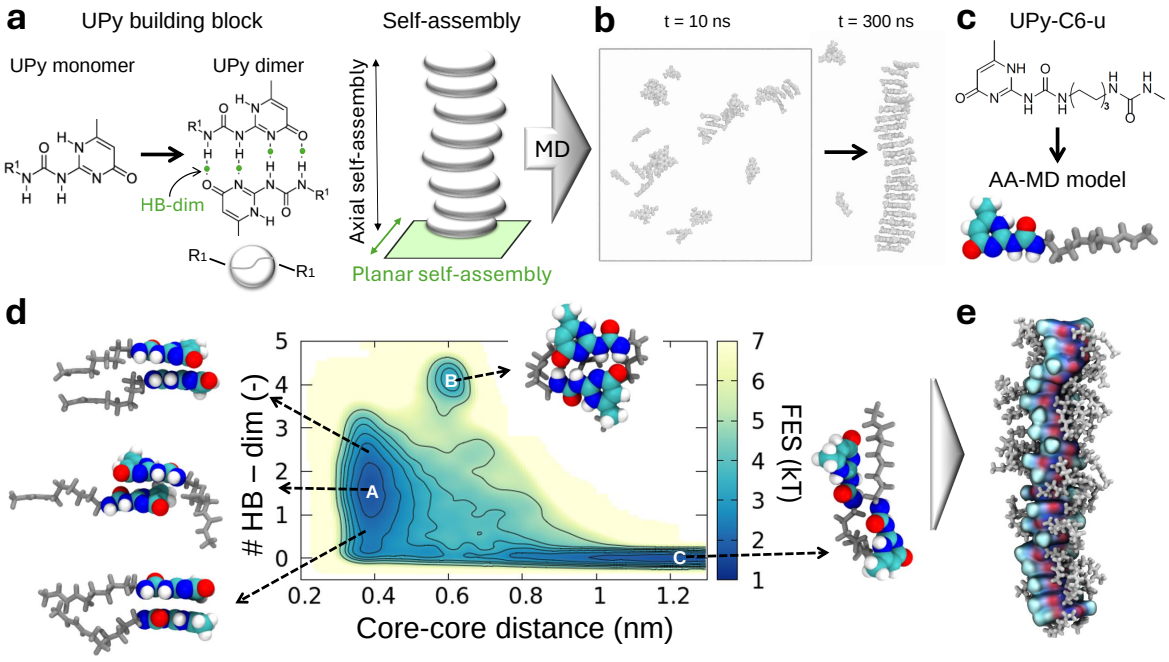

Fig. 1 Molecular Dynamics (MD) models of UPy-based building blocks. a) Left: Chemical structure of two UPy monomers forming a dimer by self-complementary quadruple hydrogen bonds (HB-dim). R_1 indicates a possible functionalization. Right: Self-assembly cartoon of UPy dimer building blocks in the axial direction, creating a polymer. b) All-Atom MD (AA-MD) simulation of (R1-free) UPy dimer self-assembly. Two MD snapshots at 10 and 300 ns are shown. c) Chemical structure and AA-MD model of UPy-C6-u monomer considered in this study. Oxygen, carbon, and hydrogen atoms of the UPy-C6-u core are colored in red, gray, and white, respectively. The side chain is in light gray. d) UPy-C6-u dimerization Free-Energy-Surface (FES) in aqueous solution obtained with Well-Tempered MetaDynamics (WT-MetaD) simulation. HB-dim and Core-core distance are selected as the WT-MetaD collective variables. A, B, and C identify three energy minima corresponding to the stacking, dimerization, and lateral assembly configurations, respectively. e) AA-MD snapshot of the pre-stacked UPy-C6-u polymer made of 20 dimers considered in this study.

liquid-phase-separation (LLPS) found in biological fibrils, collagen, and, in general, to reproduce the adaptive behavior of extracellular matrices (ECM) with tunable stiffness, dynamics, and bioactivity.[35,39,41] However, for inducing cell adhesion in hydrogel networks, tight control over multiscale dynamic processes is required[43]. Particularly, a tailored understanding is crucial for both molecular-level dynamics—such as monomer exchange within SPs—and the bulk dynamics, i.e., polymer rearrangements in hydrogels covering larger scales.

Although recent experimental studies have provided estimates for the monomer exchange rate in UPy-based SPs (10% in 1 hour)[35,43], most experimental approaches cannot resolve the molecular and submolecular mechanisms occurring in UPy-based polymers, where monomeric and oligomeric units continuously exchange, setting a supramolecular "equilibrium dynamics." This monomer exchange dynamics, on the other hand, can be well detected by multiscale molecular modeling and advanced computational methods[44–46]. In this framework, while BTA-based polymers have been largely investigated with atomistic,[47–49] higher-scale simulations,[44,50,51] and advanced ML tools,[52–54] UPy-SPs have received much less attention from computational research. Chen *et al.* used umbrella sampling technique to estimate the potential of mean forces between two interacting UPy molecules. While their work successfully highlights the role of the hydrophobic spacer in the UPy dimerization process, it does not capture the range of configurations that UPy building blocks may adopt while self-assembling. Later studies utilized atomistic and coarse-grained simulations to investigate the self-assembly mechanisms occurring in longer UPy-based polymers.[56,57] These approaches, however, are constrained by time and space limitations typical of classical MD, preventing a thorough exploration of the system's configurational space. Additionally, none of the computational studies conducted so far have investigated the essential phenomenon of monomers' exchange within and outside their self-stacking structure at the basis of bioinspired properties such as self-healing and reconfiguration.

Here we present a computational work where MD, enhanced sampling approaches, and ML techniques are integrated to provide an overview of the structural and dynamics features of UPy-SPs in water. In this study, the UPy core is functionalized with short carbon spacers terminating with a urea moiety (UPy-C6-u in Fig. 1c). The UPy core forms dimers through quadruple hydrogen bonding, and the hierarchical growth is also driven by bifurcated hydrogen bonds of the urea group flanking the alkyl spacer.[58,59] Starting from pre-assembled UPy polymers—based on literature data and preliminary MD indications—we first investigate the structural properties of these UPy stacks, assessing their size-dependent stability. The dynamics of monomer exchange is then studied via Infrequent Well-Tempered Metadynamics (WT-MetaD) simulations,[60] which accelerate the rupture of the dimerization hydrogen bonds across the supramolecular structure. Second, we employ data-driven analyses[61,62] to detect key dynam-

View Article Online
DOI: 10.1039/D5TB01272D

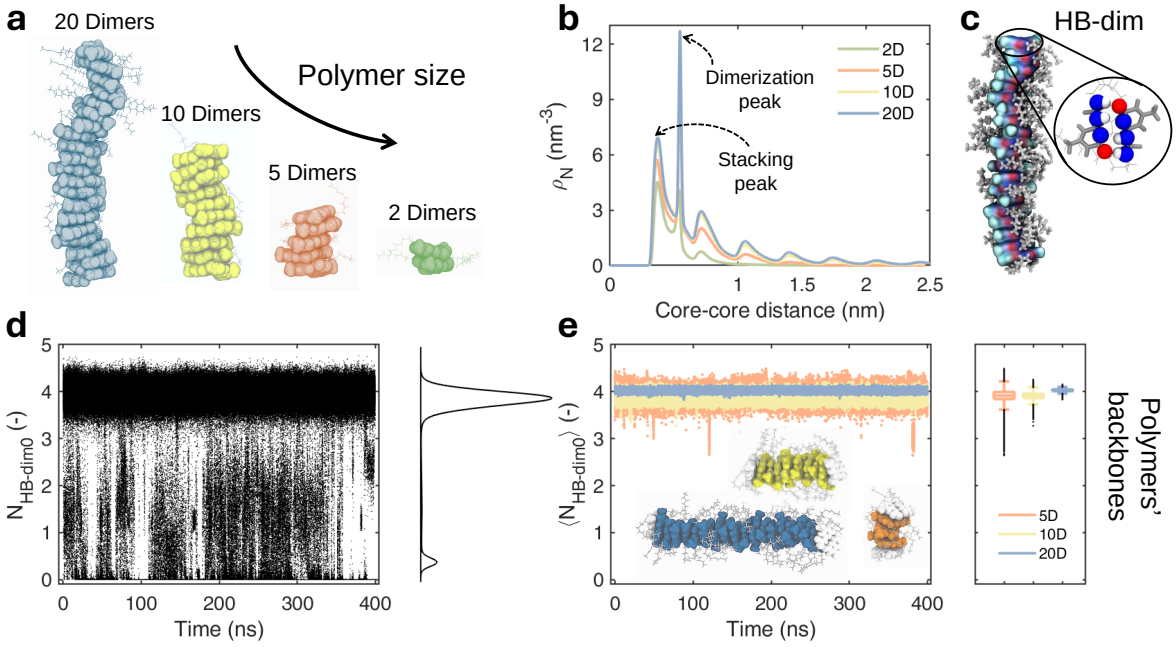

Fig. 2 Structural analyses of UPy-C6-u stacks. a) AA-MD snapshots of four UPy-C6-u pre-stacked polymers as a function of assembling dimers: 20, 10, 5, and 2 Dimers (D). b) Radial Distribution Function (RDF) computed on each UPy-C6-u monomer forming the four polymers in a). Blue, yellow, orange, and green RDFs identify the 20D, 10D, 5D, and 2D polymers. c) AA-MD snapshot of the 20D polymer. The atoms chosen to account for the number of dimerization hydrogen bonds ($HB-dim$) are displayed as colored spheres in the zoom. d) Number of initial $HB-dim$ ($N_{HB-dim0}$) time series, computed on each dimer forming the polymers in a) through the 400 ns equilibrated MD simulations in water. The Kernel Density Estimation (KDE) profile of all $HB-dim0$ data is plotted on the right-hand side. e) Number of $HB-dim0$ averaged over all the dimers in the polymer backbones (tips excluded) reported in a), as a function of t along the 400 ns-long MD trajectories. The $\langle N_{HB-dim0} \rangle$ time series are colored according to the stacks size; the time-averaged values of $\langle N_{HB-dim0} \rangle$ are displayed in the boxplot on the right-hand side.

ical environments, which reveal the mechanisms of monomers' exchange within the stacking supramolecular polymer. Finally, we also provide insights on the monomer exchange dynamics occurring between bundled UPy polymers, the typical higher-level structure detected in experiments[35,43,58,63]. This study provides solid guidelines to describe the structure and dynamics of UPy-based assemblies in water, allowing us to gather useful indications on how the molecular structure of the system relates to the supramolecular dynamics and, subsequently, to the bioinspired properties of the material[35,43,59].

1 Results

1.1 Structural analysis of UPy-C6-u polymers

By using All-Atom MD (AA-MD) simulations, we here describe the key physical and chemical mechanisms determining the structural stability and dynamic features of supramolecular UPy-based polymers. UPy building blocks dimerize in water, forming four complementary hydrogen bonds, and then grow orthogonally via π-π stacking, building 1D polymers (Fig. 1a). Such 1D dimer stacks then interact with each other, aggregating in fibers, which in turn form the bundle network that constitutes the supramolecular material. Such a hierarchical self-assembly process is here explored with atomistic detail by using AA-MD simulations of R_1-free (i.e., without side-chain R_1) UPy monomers. One single stack having such a stacked-dimer hierarchical structure is spontaneously formed after 300 ns-long MD simulation, starting from a suspension of 42 dispersed UPy monomers (Fig. 1b). This outcome confirms that the combination of hydrogen bonds and π-π interactions governs the mono-directional stacking of UPy cores. However, due to this high aggregation propensity, it is essential to enhance the water solubility and prevent the solution precipitation. Adding hydrophobic and hydrophilic side chains, i.e., functional R_1 groups, to the UPy core is a strategy to promote self-assembly in water and tune the resulting properties.

Building on experimental studies,[58,59] here we select a relatively simple molecular design for the UPy-based motif, namely including one hydrophobic spacer with 6 carbon atoms (C6-spacer) and one urea terminal (the chemical structure of the UPy-C6-u monomer and the relative all-atom model are in Fig. 1c). This monomeric structure adds the complexity of an interacting side-chain without overly increasing the simulation times required to capture the monomer exchange dynamics across the supramolecular structure. Unlike the self-aggregation of UPy R_1-free monomers (Fig. 1a), it is challenging to observe the spontaneous and ordered assembly of UPy-C6-u within the timescales accessible through AA-MD. Therefore, our computational protocol includes the setup of pre-stacked UPy-C6-u polymers based on the configurational guidelines emerging from the analysis of UPy dimerization Free-Energy Surface (FES). To estimate the FES we adopted Well-Tempered MetaDynamics,[64] (WT-MetaD), choosing the number of dimerization hydrogen bonds, $HB-dim$, and the core-core distance as collective variables (see the Method sec-

View Article Online
DOI: 10.1039/D5TB01272D

tion). The resulting FES (Fig. 1d) exhibits three minima, **A**, **B**, and **C**, corresponding to the most probable configurations retained by two UPy-C6-u monomers in aqueous solution. The first minimum, **A**, represents the two-monomer-stacking arrangement in the orthogonal direction, having a core-to-core distance of ≈ 0.4 nm in conjunction with the formation of ≈ 2 HB − dim. The second minimum, **B**, corresponds to the dimer assembly driven by self-complementary quadruple hydrogen bonding in a DDAA pattern, i.e., HB − dim = 4, associated to a core-to-core distance of ≈ 0.6 nm, matching with earlier experimental results[63]. Finally, the third minimum **C**, lays down in the phase space of zero HB − dim and core-core distances around ≈ 1.2 nm. The MD representative snapshot of **C** state (Fig. 1d) reveals that the UPy-C6-u monomers are bound head-to-tail, held together by urea-core interactions. This suggests a possible arrangement of the inter-polymer aggregation within a larger self-assembly. Based on these favorable dimer configurations and on the experimental evidence of supramolecular polymer structures,[32–34] we arranged UPy-C6-u monomers in stacks formed by pre-assembled dimers, and we tested the stability of such structures via AA-MD (Fig. 1e).

The structural stability and supramolecular dynamics of the pre-assembled UPy-C6-u polymers are investigated by simulating, for 400 ns in aqueous solution, 4 polymers of distinct sizes, i.e. 2, 5, 10 and 20 dimers (Fig. 2a). The resulting MD trajectories are firstly analyzed by computing the radial distribution function (RDF) among all monomers, considering the distance between the UPy cores' center of mass. Regardless of stacks' length, the RDF profiles show multiple regular peaks obtained at increased core-core distance (Fig. 2b). For each system, the first peak occurs at 0.37 nm, which approximately corresponds to the position of the free energy minimum **A** (Fig. 1d). This peak therefore identifies the first neighbors along the stacking direction. The next peak, located at ≈ 0.6 nm, corresponds to the monomer-core distance relative to the dimer formation, as confirmed by the free energy landscape in Fig. 1d (**B** minimum). The subsequent lower and broader peaks include both the higher-order stacking and dimerization configurations (that are degenerate at this order). We observe that longer polymers exhibit higher peaks. Considering that the reported RDF is normalized by the number of monomers, we expect that the purely stacking peaks increase with polymer size due to the higher statistics of neighbors. However, the same does not hold for the dimerization peak, and its size dependence is evidence of dimer stability in longer polymers. We also found that the probability of a UPy-C6-u dimer to be in a perfect planar orientation is higher in a longer stack (20D) as compared to a short one (2D) (Fig. S1 in SI). These elements indicate that an ordered, planar dimer conformation is more likely in longer SPs, suggesting the cooperativity in the supramolecular polymerization of UPy-C6-u.

1.2 Monomer exchange dynamics in UPy-C6-u polymers

The dynamics of supramolecular polymers is directly linked to the stability of their reversible bonds, which regulate the formation and resolution of structural defects—fundamental to self-healing mechanisms. In other words, strong non-covalent bonds among the UPy-C6-u monomers tend to prevent their reshuffling and thus the overall dynamics. In UPy-C6-u, the fibrillar structure rests both on the HB − dim forming the dimers and on the π-π stacking that fuels polymer elongation. Therefore, to give quantitative insights into the dynamic nature of our UPy-C6-u polymers, we first focused on the reversibility of HB − dim as source of structural defects. We calculated how many of the 4 initial dimerization H-bonds (HB − dim0) are preserved by each monomer along the MD trajectories of the polymer chains (Fig. 2a and zoom of Fig. 2c). As a result, the number of HB − dim0, i.e. $N_{HB-dim0}$, of each monomer is equal to 4 at the beginning, and it decreases if the original HB − dim conformation is disrupted, as shown by the $N_{HB-dim0}$ time series (Fig. 2d). As discussed in the Methods section, the estimated HB − dim0 intrinsically include spurious interactions that generate the fluctuations seen in the profiles (Fig. 2d). We employed relative Kernel Density Estimation (KDE) to highlight the main features of the $N_{HB-dim0}$ distribution over the MD data. In particular, the KDE evidences the presence of two main peaks: The largest peak contains those dimers for which the $N_{HB-dim0}$ fluctuates around 4, corresponding to the full starting HB − dim (the self-complementary dimer assembly shape shown in Fig. 2c); the second peak indicates that a sample of dimers breaks, forming structural defects. Based on previous results on BTA supramolecular polymer dynamics,[44] we then differentiate how many $N_{HB-dim0}$ are preserved between tip and backbone dimers to identify which ones contribute to the formations of defects. Thanks to this classification, we notice that the HB − dim0 in the backbone are overall very stable, oscillating within the main peak of the KDE distribution ($N_{HB-dim0} \sim 4$ in Fig. 2e), thereby demonstrating that dimer rupture events do not occur in the backbone. On the contrary, the $N_{HB-dim0}$ computed for specific tip dimers fluctuate from 4 to 0, revealing that full dimer breakage takes place here. In the cases of polymers formed by 20, 10, and 5 dimers, the KDE distribution of the tips (Fig. 3a) is also featured by two main peaks, indicating that intermediate states with $N_{HB-dim0}$ from 1 to 3 are more ephemeral. In contrast, the 2D polymer, where all four monomers are formally part of the tips, displays a constantly fluctuating $N_{HB-dim0}$, alternating defect generation and self-healing, with intermediate dimerization states. Therefore, the 2D polymer, where distinction between the backbone and tips is absent, shows a substantially higher monomer exchange.

The unique behavior of dimerization H-bonds depending on whether the dimers are arranged as tip or backbone suggests a crucial role of the physical environment in which the defects occur, specifically the key contribution from the competitive solute-solvent interaction. This is validated by a clear correlation between the time-averaged $N_{HB-dim0}$ and the Solvent-Accessible Surface Area (sasa) associated to each monomer: the monomers that exhibit a larger contact with water (higher sasa) are more prone to dimer disassembly (lower $\langle HB\text{-}dim \rangle$) and hence to the defect formation (Fig. 3b). The results achieved at this stage definitely confirm that the physical-chemistry source behind a defect generation in the UPy-C6-u polymers is the hydration; nevertheless, the limited time and space scales considered in these standard MD simulations make it difficult to generalize these findings.

View Article Online
DOI: 10.1039/D5TB01272D

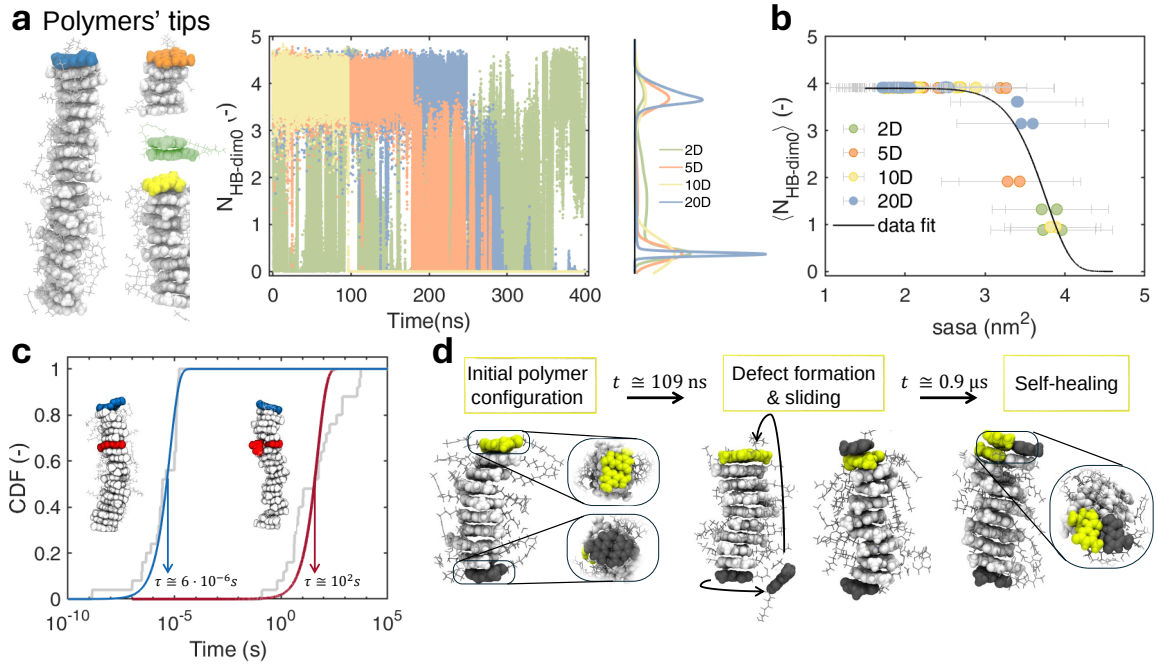

Fig. 3 Dynamics of UPy-C6-u polymers. a) Number of $HB-dim0$ time series relative to the dimers at the tips of differently sized polymers (the considered tips are colored in the polymer snapshots on the left). The KDE highlights the distribution features for the considered tip dimers, showing the breakage of the initial HBs. b) Correlation between the time-averaged $N_{HB-dim0}$ computed on each UPy-C6-u monomer forming the polymers and its associated sasa. The data points are colored based on polymer size, while a nonlinear fitted curve is shown with a black line. c) Cumulative Distribution Functions (CDF) of the defect creation times (i.e., dimer rupture) resulting from 30 repetitions of infrequent WT-MetaD. Two distributions are shown, either involving a tip dimer (blue fitting curve) or a backbone dimer (red fitting curve). τ is the characteristic time-scale extracted via CDF fitting. d) AA-MD snapshots of the 10D polymer in 1 μs-long MD simulation. Initial tip dimers are highlighted in dark gray and yellow, while the polymer backbone is in light gray. The MD snapshots highlight the defect formation, monomer sliding, and self-healing process involving the system.

For this reason, we used the infrequent WT-MetaD technique to stimulate the rupture of a dimer bond in a 20D polymer. This allows estimating the characteristic time associated to defect generation from either backbone or tip dimers. This analysis shows that the formation of a defect from a tip dimer (Fig. 3c, blue curve) is 7 orders of magnitude faster than the formation of a defect from a backbone dimer (Fig. 3c, red curve). Such a difference suggests that tip dimers also dominates real systems where the tip-to-backbone ratio is lower than in our model polymers.

Although the investigation around the $HB-dim0$ allows the detection of initial dimer disassembly and defect formation, in general, such an analysis is not suitable to capture the self-healing events, as $N_{HB-dim0}$ cannot detect the dimerization of monomers not coupled in the starting polymer (see also discussion in the Methods section). This is, for example, the case reported in Fig. 3d where we compare some configurations of the 10D polymer along 1 μs of MD. After 100 ns, one of the tip dimers (in dark gray in Fig. 3d) disassembles, and one of the two unbound monomers slides along the polymer, stacking on the opposite end. Approaching to 1 μs, this monomer self-assembles with one of the monomers at the tip (in yellow), forming 4 complementary $HB-dim$. This is an example of defect self-healing, which characterizes the properties of this system. A similar dynamics also occurs in the 20D (Fig. S2 in SI). To systematically investigate the mechanisms of defect formation and self-healing, we analyze the dynamics of the system from a different viewpoint. Recently developed descriptors, coupled with ML tools, have been shown to accurately capture diverse structural environments within a self-assembly, including the probability of building blocks to transfer among the detected domains.[52,65] Dynamic environments, on the other hand, have been directly extracted by using descriptors pointing out the time evolution of neighborhood environments.[53,61,62,66] In the latter context, Time Smooth Overlap of Atomic Position (τSOAP).[61] focuses on the variations in the supramolecular structure of the system along the MD trajectory. More in detail τSOAP provides a scalar quantity (normalized from 0 to 1) that identifies the rate of structural rearrangements that occurred in the surroundings of selected *centers*. These *centers* are identified with specific groups, defining the main interactions between building blocks, thus providing a useful classification of the monomer exchange dynamics in supramolecular structures.[61] In our case, we locate the *centers* of τSOAP calculation at the center of mass of the 4 atoms forming the $HB-dim$ so that, as shown in our previous results, the arrangement of different *centers* is informative not only about the formation of dimers but also about the stacking. With this definition, τSOAP captures the dynamic arrangement of the UPy-C6-u interacting groups (see the Method section for further details). Analyzing the statistics resulting from the time evolution of τSOAP for each monomer, we can extract a classification of the main dynamic domains featuring the polymer.

We thus simulate the 20D-polymer system for 1.6 μs, computing the τSOAP descriptor for each of the 40 monomers along the

View Article Online
DOI: 10.1039/D5TB01272D

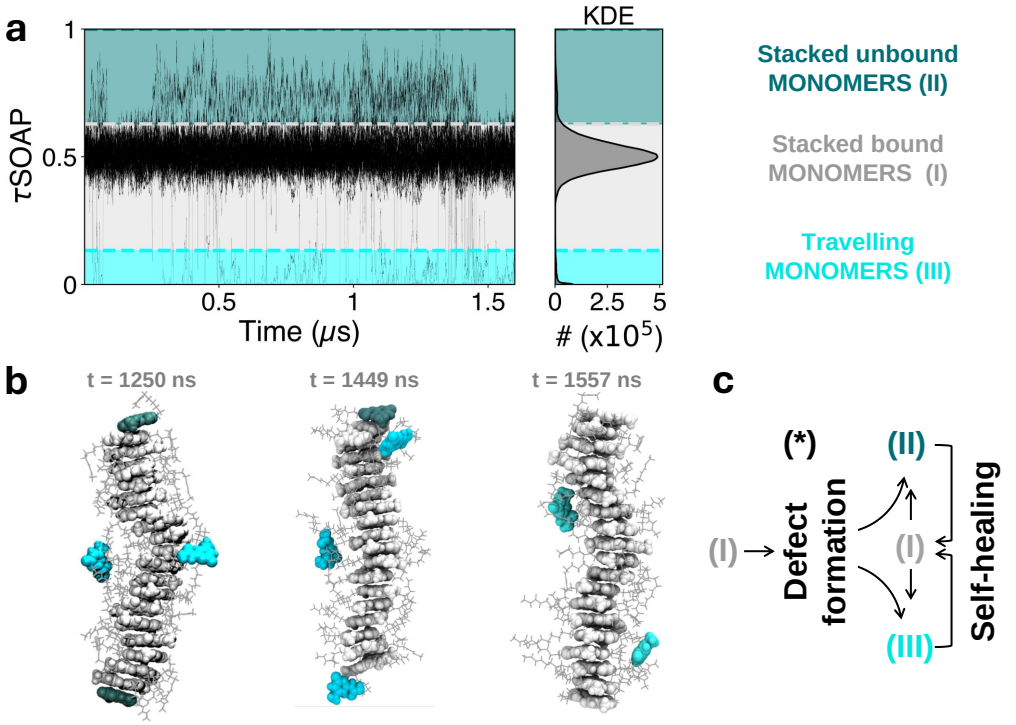

Fig. 4 Monomer exchange pathway. a) τSOAP time series computed on the interacting *centers* of each monomer of the 20D UPy-C6-u polymer in Fig. 2a, along a 1.6 μs MD. The KDE distribution of the data is shown on the right. The cluster analysis carried out on the τSOAP data detects three domains: I) stacked bound monomers (light gray), II) stacked, unbound monomers (teal), and III) travelling monomers (cyan). b) Three emblematic MD snapshots of the 20D polymer, where monomers are colored according to the domains identified. c) Scheme of possible monomer exchange pathways: Starting from an ideal configuration of stacked dimers into a polymer (I), a defect formation induces either stacked unbound (II) or travelling monomers (III), which eventually may exchange their configurations or self-heal by restoring a new stacked dimer (I).

MD trajectory. The time evolution of τSOAP, together with its KDE, shows a data region particularly dense around $\tau\text{SOAP} = 0.5$, identifying the most probable dynamic state, while sparse fluctuations arise both below and above this dense data distribution (Fig. 4a). A proper cluster analysis of these data series detects the presence of three domains, one corresponding to the more dense data region and the other two above and below, respectively. Such cluster analysis also allows us to associate the identified dynamic domains to monomers that are found in a different structural state: (I) the stacked bound monomers, which form the most populated cluster characterized by an intermediate value of τSOAP, i.e., a moderate rate of structural rearrangement of the environment (light gray cluster in Fig. 4a); (II) the stacked unbound monomers, which manifest the highest dynamics in terms of neighborhood reconfiguration (teal area in Fig. 4a); and (III) the monomers dissolved in solution, or sliding along the polymer surface, which correspond to the lowest values of τSOAP (cyan area in Fig. 4a). In these third configurations, the interacting *centers* are far from the others, thus, their environment appears static from our definition of τSOAP (cyan region in Fig. 4a). The MD snapshots of three 20D polymers are reported with the monomers' colors corresponding to the classification in Fig. 4a (Fig. 4b). In this graphical representation, the ideal assembly configuration (I), characterizing the bound monomers, as well as the defect events, identified as either (II) or (III) states can be clearly visualized. Based on this classification, we can now interpret the τSOAP signal relative to each monomer (*center*): The defect formation events take place when a monomer transfer occurs from I to II or from I to III—as well as self-healing events arise when a monomer moves from I or III to domain II (Fig. 4c). Fig. 5 shows some emblematic examples of monomer exchange dynamics. For instance, M1 and M2 are two tip monomers initially bound, as distinctly confirmed by their τSOAP values, averaging around 0.5 for the first 250 ns (green and purple τSOAP signals in Fig. 5b and relative MD snapshots in Fig. 5a). Then, after 250 ns, a defect forms and while M1 remains bound to the tip (with its τSOAP value transitioning to higher values, II), M2 starts sliding along the polymer (with τSOAP value shifting towards 0, III). After 1 μs, we observe a self-healing event, in which M2, which in the meanwhile has reconfigured as stacked unbound monomer (domain II), dimerizes with M40, which travels toward M2 from the other end of the polymer (the orange profile in Fig. 5b and final MD snapshot in Fig. 4a).

Overall, this second analysis also confirms that monomer exchange dynamics concentrates at the tips of the polymers, highlighting that both defect creation and self-healing preferentially occur at the ends (Fig. S2 in SI). This observation is consistent with the relatively slow dynamics of UPy-C6-u polymers detected in the experiment.

We finally explored how the monomer exchange dynamics is affected when multiple UPy-C6-u polymers (Fig. 6) interact to form fibers, typical of the UPy supramolecular structure.[35,43,58,63] We

View Article Online
DOI: 10.1039/D5TB01272D

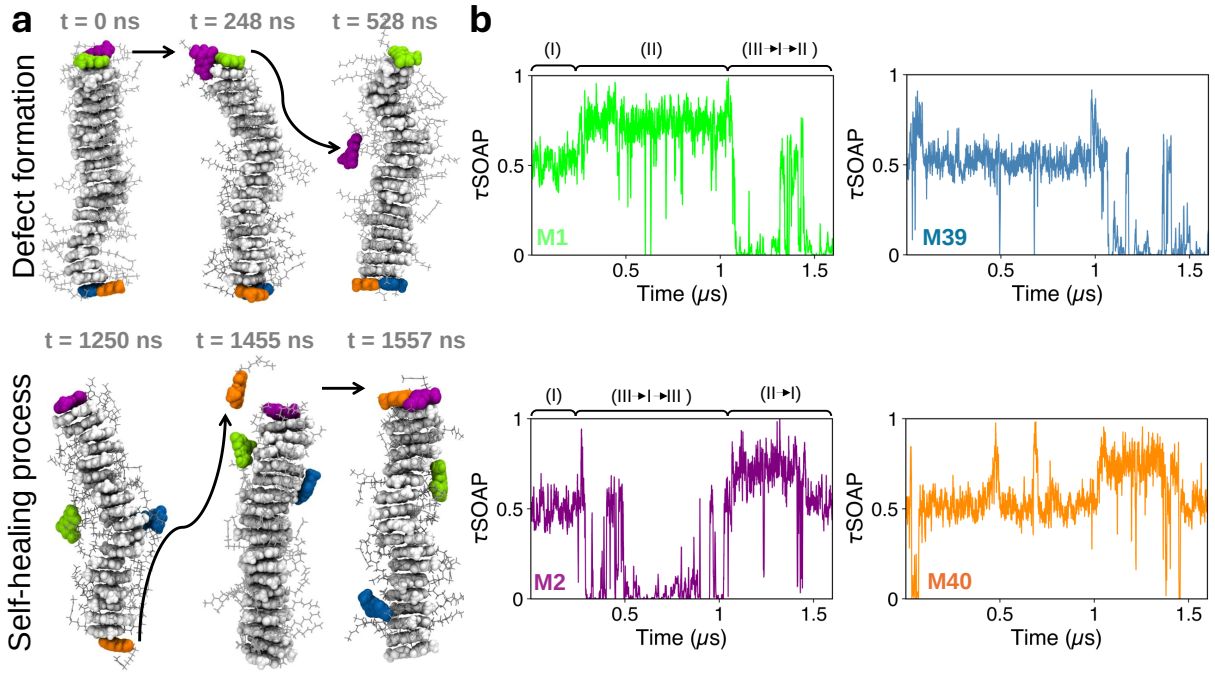

Fig. 5 Monomer exchange pathway. a) MD snapshots of the 20D polymer. The backbone is colored in light gray, while the initial tip monomers are evidenced by different colors: M1 in green, M2 in purple, M39 in blue, and M40 in orange. The disassembly of M1-M2 dimer is displayed on the top side, showing the defect formation. At 248 ns, the initial dimerization HBs break apart; then M2 starts sliding on the polymer, while M1 remains unbound. The self-healing process instead is clarified following the M40 pathway on the downside: the decisive disassembly of the M39-M40 dimer occurs at around 1 μs, then M39 starts travelling, while M40 remains stacked and unbound. At 1455 ns M40 detaches from the polymer and reaches M2 monomer, forming a new dimer. b) τSOAP time series for M1, M2, M39 and M40 as defined in a). Here, several pathways of defect creation and self-healing can be identified, clarifying the mechanisms of monomer exchange dynamics.

therefore carried out an unbiased MD simulation of three 20D polymers initially placed next to each other, following their interaction along the trajectory. As shown by the sequential snapshots reported in Fig. 6a, few events of inter-polymer exchange were captured within a 3 μs timeframe.

Entering more in depth into the inter-polymer dynamics we observe that the aggregation propensity, namely the ratio between the sasa of three ideally isolated polymers over the sasa of the assembly computed at time t, signals the tendency of the polymers to aggregate in fibers, progressively reducing their solvent exposure (Fig. 6b). This aggregation is mainly driven by side-chain interactions, as shown by the relatively small number of inter-polymer contacts formed by the core UPy motifs, i.e. excluding side-chain contacts (Fig. 6c). Interestingly, monomer exchange within the fiber occurred almost exclusively at the polymer tips. Separating the average number of inter-polymer contacts "nc" established by each tip monomer (end dimers and their first neighbors) from those established by backbone monomers, revealed a striking difference between the two. The value of tips' nc mostly fluctuates within the 40-60 range, whereas the backbone's nc mostly remains around 5 (Fig. 6c). Besides this quantitative evidence, MD snapshots visually confirm that exchanges are localized at the tips (Fig. 6a). Moreover, by performing long MD simulations (7 μs) of three infinite polymers at $T = 343$ Kelvin, we could observe that backbone exchanges are not strictly forbidden, but they are far less frequent than tip exchanges (Fig. S4). This evidence supports our interpretation of why UPy-based polymers display slower dynamics compared to other supramolecular polymers such as BTA.[35,41] Our analysis also indicates that the monomer sliding observed along the surface of an isolated chain becomes less favorable in fibers, where side-chain interactions between adjacent polymers hinder such motion. These multi-polymer simulations therefore provide valuable context for interpreting single-chain monomer exchange results in the framework of the hierarchical structures formed by UPy motifs.

Conclusions

We here report for the first time a computational MD study on the monomer exchange dynamics of UPy-C6-u supramolecular polymers in aqueous solution. In particular, we shed light on the processes of defect creation and self-healing pathways, which are key aspects for monomer motion in SPs.

First, the dimerization free energy surface between two UPy-C6-u monomers in water has been investigated to assess the supramolecular architecture of the system, based on quadruple hydrogen bonds (HB – dim) creating dimer units that stack into polymers. Structural analysis carried out on such polymers of distinct sizes has highlighted a cooperative effect, by which the quadruple HB – dim appear to be more stable in longer polymers, with subsequent increased stability of the entire structure.

The monomer exchange mechanism in UPy-based supramolecular polymers was then explored more in detail. By following

View Article Online
DOI: 10.1039/D5TB01272D

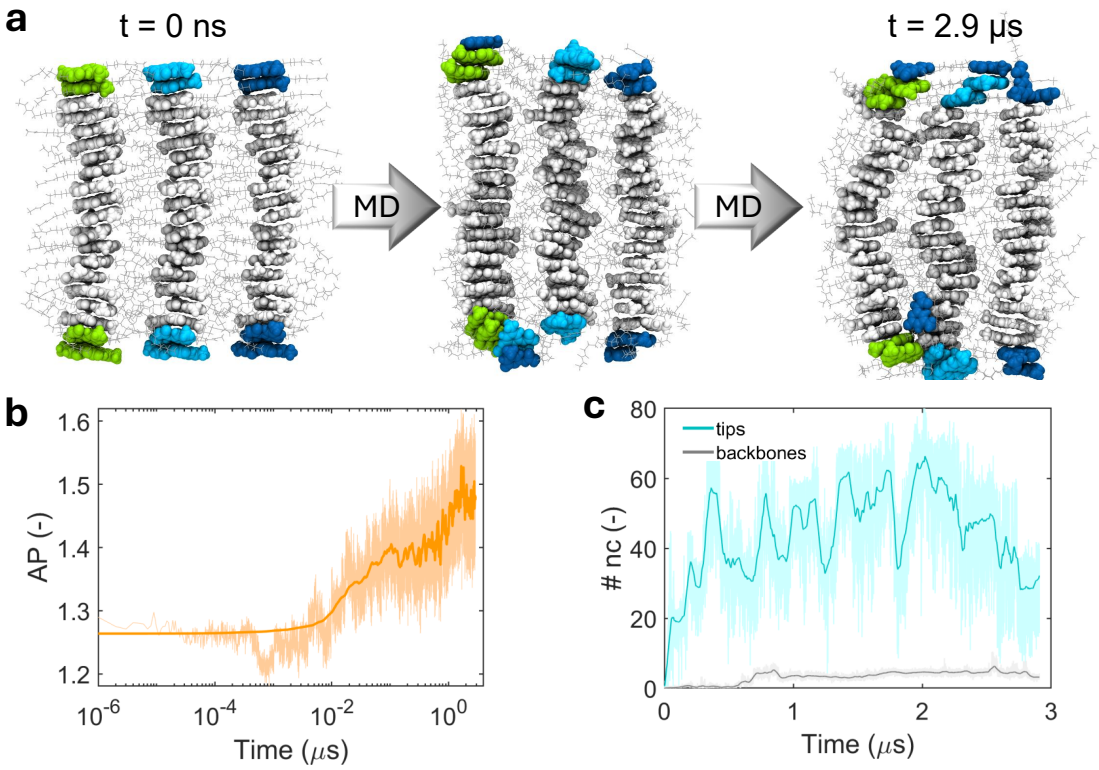

Fig. 6 Inter-polymer monomer exchange dynamics. a) Three snapshots of AA-MD simulating three parallel 20D polymers placed next to each other. Monomers initially located at the tips of each polymer, as well as the first neighbors are colored in green, cyan and blue, depending on the polymer they belong to. The other, backbone monomers are colored in gray. The inter-polymer dynamics is localized at the tips. b) Aggregation Propensity (AP, see text for the definition) of the three polymers along the AA-MD simulation. c) Average number of inter-polymer contacts per monomer (nc) in case of tips/subtips (cyan curve) and backbones (gray curve).

the initial number of HB – dim0 along MD trajectories, we found that the dimers' disassembly seen as a consistent variation of HB – dim0 involves exclusively tip monomers rather than backbone. To explain this evidence, the solvent accessible surface area was calculated for each monomer along the MD trajectory. The resulting data demonstrate a correlation between hydrogen bond breaking and monomer hydration, thereby suggesting that competitive solute-solvent interactions are the main driving force for dimer rupture, i.e. defect formation. This result is also quantitatively supported via infrequent WT-MetaD simulations, showing that dimer defect formation occurs several order of magnitude faster at the tips than in the backbone.

We then employed τSOAP[61], a recently developed descriptor of atomic environment dynamics, to obtain further insights on the most probable defect and self-healing mechanisms taking place along these polymers. Specifically, τSOAP coupled with ML tools allow classifying the different monomers according to the dynamics of their supramolecular surroundings, thereby unveiling possible pathways of monomer exchange events. We finally presented AA-MD simulations of UPy polymer fibers, showing indications on how monomer exchange dynamics takes place when multiple UPy stacks aggregate. Overall, our results show that the origin of UPy-SPs dynamics always relies on the mechanism of dimers' disassembly, which, while leading to either traveling or stacked-bound monomers (defect creation), offers a suitable local environment for self-healing (defect resolution).

In conclusion, beyond the specific case study, our combined computational approaches define a modeling strategy able to systematically investigate the hierarchical self-assembly in supramolecular systems. Although experimental techniques have made it possible to quantify the dynamics within SPs (e.g. estimating a 10% of monomer exchange per hour in UPy-SPs versus 30% – 40% per hour in BTA-SPs[35,41]), in this study we complement the experiments by unveiling the most favorable local environment for dimer breakage, the mechanism of monomer exchange, and the underlying principle of self-healing.

2 Methods

2.1 All-Atom Molecular Dynamics (AA-MD) simulations

The atomistic models of UPy-based monomers, including both UPy without functionalization and UPy-C6-u, were built with Avogadro[67] following the chemical structure of the molecules. Gaussian[68] tool, based on the HF/6-31G*, was used to estimate the generated electrostatic potential, and then the RESP[69] method was applied to obtain the partial charge distribution within the molecule. The complete parameterization was based on the General AMBER Force Field (GAFF),[70] using Antechamber.[71].

View Article Online
DOI: 10.1039/D5TB01272D

2.1.1 Self-assembly of UPy monomers

The self-assembly MD simulation of 42 no-fuctionalized UPy monomers was carried out in GROMACS 2021[72]. First, the parameterized UPy monomers were randomly dispersed in a $10 \times 10 \times 10$ nm^3 box filled with water molecules described by the TIP3P model[73] and periodic boundary conditions were applied in all box directions. The non-bonded interactions among monomers, including Van der Waals and short-range electrostatic interactions, were evaluated within a cut-off radius 1.4 nm, while for the remaining long-range interactions, a particle-mesh Ewald summation was applied to resolve electrostatics in the Fourier space. Two equilibration steps were performed to reach the thermodynamic conditions of 298 K and 10^{-5}bar Pa. The self-assembly simulation, lasting 1 μs, was performed by using the v-rescale thermostat[74] ($\tau_T = 0.1$ ps) coupled with the c-rescale barostat[75] ($\tau_p = 0.1$ ps).

2.1.2 Pre-assembled UPy-C6-u polymers

We promoted the dimerization of two UPy-C6-u monomers and their self-assembly in the axial direction, forming UPy-C6-u polymers of distinct size from 2 to 20 dimers. We studied the stability of a single UPy-C6-u polymer in aqueous solution via classical All Atom (AA) MD simulations carried out with the open-source software GROMACS 2021[72]. Each single polymer was first solvated in a $5 \times 5 \times 5$ nm^3 box filled with water molecules described by the TIP3P model[73] and periodic boundary conditions were applied in all box directions. Note that for the 20 dimer polymer, a $10 \times 10 \times 10$ nm^3 box was considered. The non-bonded interactions among monomers, including Van der Waals and short-range electrostatic interactions, were evaluated within a cut-off radius 1.4 nm, while for the remaining long-range interactions, a particle-mesh Ewald summation was applied to resolve electrostatics in the Fourier space. Our MD protocol consisted of a first step of energy minimization and two consequent equilibration steps. Initially, to reach an equilibrium temperature of 298 K, we applied the canonical ensemble (NVT) for 2 ns using a Maxwell Boltzmann speed distribution and the V-rescale thermostat[74] with $\tau = 0.1$ ps. Subsequently, we set the isothermal-isobaric (NPT) ensemble for 2 ns at an equilibrium pressure of 10^{-5}bar Pa and an equilibrium temperature of 298 K. In this step, we used the previous thermostat coupled with the c-rescale barostat[75] with a time constant of 2 ps. During the equilibration steps, the UPy-C6-u atoms were restrained in their initial positions using a harmonic potential with a force constant of 1000 kJ/mol/nm^2. Once the desired thermodynamic conditions were reached, the restraint was removed, and a 400MD run (integration step $dt = 0.002$ ps) was carried out by maintaining the temperature at 298 K with a Noose-Hoover thermostat ($\tau = 0.8$ ps) and the pressure at 10^{-5}bar Pa ($\tau = 2$ ps) by imposing the Parrinello-Rahman barostat[76] Along the MD simulation, the LINCS algorithm was employed to restrain the covalent bonds involving hydrogen atoms.

To compare the stability of the four polymers, we first analyzed the production run trajectories by computing the radial distribution function between UPy-C6-u monomers. The dimerization hydrogen bonds (HB-dim) were estimated in PLUMED 2.6.[77,78] taking into account the coordination ($R_0 = 0.12$ $D_0 = 0.27$) among the colored atoms in the zoom of Fig. 2c. Note that, while performing this estimation, we kept the initial dimer configuration through the complete trajectory analysis. The τSOAP descriptor was instead applied to each monomer of the 20D polymer, and specifically on the center of mass of the oxygen and nitrogen atoms involved in possible dimerization HBs (zoom in Fig. 2c). Thus, for each individual *center* i, τSOAP$_i$(t) monitors the $i-th$ local environment changes in terms of neighbor monomers' arrangement along the trajectory, ranging from 0 to 1 for static to highly dynamic neighborhoods, respectively. The instantaneous τSOAP value is defined as:

$$\tau SOAP_i^{t+\Delta t} \propto \sqrt{2 - 2\mathbf{p}_i^t \mathbf{p}_i^{t+\Delta t}}, \quad (1)$$

where $\mathbf{p}_i^t$ is the full SOAP feature vector associated to the i-th individual *center* within a certain cutoff neighborhood (r_{cut}) at the time step t, as described in detail in Ref.[61]. Here, $r_{cut} = 0.6$ nm was employed. In brief, τSOAP$_i$(t) tracks the variations of the i-th SOAP vector over time, that is, to what extent the molecular environment related to each *center* changes at every consecutive time interval Δt in terms of SOAP power spectrum. The unsupervised clustering algorithm of Gaussian Mixture Models[79] was finally adopted to rationalize the data and to identify the dominant molecular environments in the polymer. Similar outcomes are also achieved by applying the recent LEAP analysis,[62] combining LENS[53] and τSOAP descriptors (Fig. S3 in SI).

2.2 UPy-C6-u dimerization Free Energy Surface (FES)

To explore the free energy surface (FES), which shows the thermodynamic phase space of two UPy-C6-u monomers interacting in aqueous solution, we performed extensive 355 ns-long Well-Tempered MetaDynamics (WT-MetaD) simulations.[64] We selected as collective variables (CVs) (i) HB-dim ($R_0 = 0.12$ $D_0 = 0.27$) ns and (ii) the core-core distance (see Fig. 1d). The latter CV represents the distance between the center of mass of the two UPy-C6-u cores. Note that the coordination number was computed as implemented in PLUMED 2.6.[77,78] We chose 10 as a bias factor with an initial Gaussian height of 1.5 kJ mol^{-1}, and a width of 0.5 nm for both the distance and the coordination number, respectively. The Gaussian deposition rate was set to 5000 MD $step^{-1}$, i.e., every 10 ps. After reaching convergence, we reweighted the FES using the Tiwary-Parrinello estimator[80] on the same CVs. The WT-MetaD simulations were performed using GROMACS 2021.[72] and PLUMED 2.6.[77,78]

2.3 Infrequent WT-MetaD simulations

The formation of defects along the polymer is a rare event in the timescales effectively accessible using atomistic models. As validated by some computational studies, the real (unbiased) dynamics of an event is related to the transition time associated with events activated by infrequent WT-MetaD simulations (biased dynamics).[60,80,81] This approach is particularly convenient as it allows one to directly extract information on the kinetics of the activated transition from the biased WT-MetaD simulations. Adapting this approach, we calculated the characteristic timescales, τ, for defect formation both within the backbone and on the tips of the

View Article Online
DOI: 10.1039/D5TB01272D

20D polymer. In particular, we run multiple infrequent WT-MetaD simulations where the systems undergo a transition from HB-dim = 4 to HB-dim = 0. The unbiased transition time (t) of each transition can be calculated from each WT-MetaD run as:

$$t = t_{WT-MetaD}\langle e^{\beta V(s(R,t)}\rangle_{WT-MetaD}; \quad (2)$$

where, $V(s(R),t)$ is the time-dependent bias, the exponential (brackets) is averaged over the WT-MetaD run, and β is $kT^{-}1$. The characteristic time scale, τ, of defect formation is then calculated by fitting the cumulative distribution function (CDF) with a Poisson-like cumulative probability:

$$CDF = 1 - e^{-\frac{1}{\tau}}; \quad (3)$$

Fig. 2d reports the CDF profiles of the defect formation at the polymer tip (blue curve), and backbone (red curve).

Author contributions

C.P. and A.C. designed the setup and the computational framework. L.R. and P.D. provided the case study. A.C. and C.C. carried out the simulations and the postprocessing of the data. All the authors worked on the interpretation of the results. C.P. supervised the project. All the authors wrote and approved the final manuscript.

Conflicts of interest

There are no conflicts to declare.

Data availability

The data supporting this article have been included as part of the Supplementary Information.

Acknowledgements

The authors acknowledge the computational resources provided by the Swiss National Supercomputing Center (CSCS). P.D. and L.R. acknowledge support from the Dutch Ministry of Education, Culture, and Science (gravitation programs 024.003.013 and 024.005.020), an NWO VICI grant from the Netherlands Organization for Scientific Research (NWO, VI.C.222.088), and the European Union's Horizon research and innovation program under grant agreement 101079482 ('SUPRALIFE').

References

1 I. I. Cisse, I. Izeddin, S. Z. Causse, L. Boudarene, A. Senecal, L. Muresan, C. Dugast-Darzacq, B. Hajj, M. Dahan and X. Darzacq, *Science*, 2013, **341**, 664–667.

2 G. Askarieh, M. Hedhammar, K. Nordling, A. Saenz, C. Casals, A. Rising, J. Johansson and S. D. Knight, *Nature*, 2010, **465**, 236–238.

3 D. Son and Z. Bao, *ACS Nano*, 2018, **12**, 11731–11739.

4 Y. Li, J. Zhu, Z. Zhang, J. Wei, F. Wang, G. Meisl, T. P. Knowles, E. H. Egelman and F. A. Tezcan, *Nature Chemical Biology*, 2025, 1–11.

5 H. Shen, E. M. Lynch, S. Akkineni, J. L. Watson, J. Decarreau, N. P. Bethel, I. Benna, W. Sheffler, D. Farrell, F. DiMaio *et al.*, *Nature Nanotechnology*, 2024, 1–6.

6 W. Zhu, H. Wang, B. Feng, G. Liu, Y. Bian, T. Zhao, Q. Wang and X. Weng, *Advanced Science*, 2025, 2406479.

7 M. J. Webber and M. W. Tibbitt, *Nature Reviews Materials*, 2022, **7**, 541–556.

8 A. Bayón-Fernández, A. Méndez-Ardoy, C. Alvarez-Lorenzo, J. R. Granja and J. Montenegro, *Journal of Materials Chemistry B*, 2023, **11**, 606–617.

9 T. Aida, E. Meijer and S. Stupp, *Science*, 2012, **335**, 813–817.

10 Y. Cheng, E. Hirano, H. Wang, M. Kuwayama, E. W. Meijer, H. Huang and T. Aida, *Science*, 2024, **386**, 875–881.

11 I. Insua, A. Cardellini, S. Díaz, J. Bergueiro, R. Capelli, G. M. Pavan and J. Montenegro, *Chemical Science*, 2023, **14**, 14074–14081.

12 I. Insua and J. Montenegro, *Journal of the American Chemical Society*, 2019, **142**, 300–307.

13 B. Zhu, Y. Cai, L. Zhou, L. Zhao, J. Chen, X. Shan, X. Sun, Q. You, X. Gong, W. Zhang *et al.*, *Nature Communications*, 2025, **16**, 687.

14 S. Bernhard and M. W. Tibbitt, *Advanced Drug Delivery Reviews*, 2021, **171**, 240–256.

15 A. Cardellini, F. Jiménez-Ángeles, P. Asinari and M. Olvera de la Cruz, *ACS nano*, 2021, **15**, 16139–16148.

16 J. F. van Sprang, J. G. Aarts, M. G. Rutten, L. Rijns, B. M. Tiemeijer, M. J. Schotman and P. Y. Dankers, *Advanced Functional Materials*, 2024, **34**, 2404786.

17 C. Zhao, X. Li, X. Han, Z. Li, S. Bian, W. Zeng, M. Ding, J. Liang, Q. Jiang, Z. Zhou *et al.*, *Nature Communications*, 2024, **15**, 1488.

18 N. T. P. Vo, T. U. Nam, M. W. Jeong, J. S. Kim, K. H. Jung, Y. Lee, G. Ma, X. Gu, J. B.-H. Tok, T. I. Lee *et al.*, *Nature Communications*, 2024, **15**, 3433.

19 Z. Lei and P. Wu, *Nature communications*, 2018, **9**, 1134.

20 C. Shen, X. Qiu, P. Zhang, J. Liu, Z. Zhang, B. Dong, H. Liu, C. Huang, J. Huang and X. Cui, *Chemical Engineering Journal*, 2025, **504**, 158709.

21 H. Zhang and Z. Guo, *Nano Today*, 2023, **51**, 101933.

22 S. Cantekin, T. F. de Greef and A. R. Palmans, *Chemical Society Reviews*, 2012, **41**, 6125–6137.

23 P. Besenius, G. Portale, P. H. Bomans, H. M. Janssen, A. R. Palmans and E. Meijer, *Proceedings of the National Academy of Sciences*, 2010, **107**, 17888–17893.

24 A. Demenev, S. H. Eichhorn, T. Taerum, D. F. Perepichka, S. Patwardhan, F. C. Grozema, L. D. Siebbeles and R. Klenkler, *Chemistry of Materials*, 2010, **22**, 1420–1428.

25 X. Guo, S. Wang, V. Enkelmann, M. Baumgarten and K. Müllen, *Organic Letters*, 2011, **13**, 6062–6065.

26 R. M. Da Silva, D. Van Der Zwaag, L. Albertazzi, S. S. Lee, E. Meijer and S. I. Stupp, *Nature communications*, 2016, **7**, 11561.

27 H. Cui, M. J. Webber and S. I. Stupp, *Peptide Science: Original Research on Biomolecules*, 2010, **94**, 1–18.

28 M. P. Hendricks, K. Sato, L. C. Palmer and S. I. Stupp, *Accounts of chemical research*, 2017, **50**, 2440–2448.

29 S. A. H. Jansen, E. Weyandt, T. Aoki, T. Akiyama, Y. Itoh,

View Article Online
DOI: 10.1039/D5TB01272D

G. Vantomme, T. Aida and E. W. Meijer, *Journal of the American Chemical Society*, 2023, **145**, 4231–4237.

30 S.-P. Wang, W. Lin, X. Wang, T.-Y. Cen, H. Xie, J. Huang, B.-Y. Zhu, Z. Zhang, A. Song, J. Hao *et al.*, *Nature communications*, 2019, **10**, 1399.

31 E. Weyandt, L. Leanza, R. Capelli, G. M. Pavan, G. Vantomme and E. Meijer, *Nature Communications*, 2022, **13**, 248.

32 R. P. Sijbesma, F. H. Beijer, L. Brunsveld, B. J. B. Folmer, J. H. K. K. Hirschberg, R. F. M. Lange, J. K. L. Lowe and E. W. Meijer, *Science*, 1997, **278**, 1601–1604.

33 F. H. Beijer, R. P. Sijbesma, H. Kooijman, A. L. Spek and E. W. Meijer, *Journal of the American Chemical Society*, 1998, **120**, 6761–6769.

34 P. Y. Dankers, M. C. Harmsen, L. A. Brouwer, M. J. Van Luyn and E. Meijer, *Nature materials*, 2005, **4**, 568–574.

35 L. Rijns, J. W. Peeters, S. I. S. Hendrikse, M. E. J. Vleugels, X. Lou, H. M. Janssen, E. W. Meijer and P. Y. W. Dankers, *Chemistry of Materials*, 2023, **35**, 8203–8217.

36 R. E. Kieltyka, A. C. H. Pape, L. Albertazzi, Y. Nakano, M. M. C. Bastings, I. K. Voets, P. Y. W. Dankers and E. W. Meijer, *Journal of the American Chemical Society*, 2013, **135**, 11159–11164.

37 D. J. Wu, M. G. T. A. Rutten, J. Huang, M. J. G. Schotman, J. F. van Sprang, B. M. Tiemeijer, G. M. ter Huurne, S. P. W. Wijnands, M. Diba and P. Y. W. Dankers, *Macromolecules*, 2024, **57**, 6606–6615.

38 L. Rijns, H. Duijs, R. P. M. Lafleur, R. Cardinaels, A. R. A. Palmans, P. Y. W. Dankers and L. Su, *Biomacromolecules*, 2024, **25**, 4686–4696.

39 H. Fu, J. Huang, J. J. van der Tol, L. Su, Y. Wang, S. Dey, P. Zijlstra, G. Fytas, G. Vantomme, P. Y. Dankers *et al.*, *Nature*, 2024, **626**, 1011–1018.

40 A. F. Vrehen, J. F. van Sprang, M. J. Schotman and P. Y. Dankers, *Materials Today Bio*, 2024, **26**, 101021.

41 L. Rijns, M. B. Baker and P. Y. W. Dankers, *Journal of the American Chemical Society*, 2024, **146**, 17539–17558.

42 C. M. Wallace, M. M. Rovers, R. Bellan, M. G. Rutten, A. Seddon, M. J. Dalby, P. Y. Dankers and D. J. Adams, *Journal of Materials Chemistry B*, 2024, **12**, 9283–9288.

43 L. Rijns, M. G. T. A. Rutten, R. Bellan, H. Yuan, M. L. Mugnai, S. Rocha, E. del Gado, P. H. J. Kouwer and P. Y. W. Dankers, *Science Advances*, 2024, **10**, eadr3209.

44 A. L. de Marco, D. Bochicchio, A. Gardin, G. Doni and G. M. Pavan, *ACS nano*, 2021, **15**, 14229–14241.

45 C. Perego, L. Pesce, R. Capelli, S. J. George and G. M. Pavan, *ChemSystemsChem*, 2021, **3**, e2000038.

46 M. Crippa, C. Perego, A. L. de Marco and G. M. Pavan, *Nature Communications*, 2022, **13**, 2162.

47 K. K. Bejagam, G. Fiorin, M. L. Klein and S. Balasubramanian, *The Journal of Physical Chemistry B*, 2014, **118**, 5218–5228.

48 M. Garzoni, M. B. Baker, C. M. A. Leenders, I. K. Voets, L. Albertazzi, A. R. A. Palmans, E. W. Meijer and G. M. Pavan, *Journal of the American Chemical Society*, 2016, **138**, 13985–13995.

49 M. B. Baker, L. Albertazzi, I. K. Voets, C. M. Leenders, A. R. Palmans, G. M. Pavan and E. Meijer, *Nature communications*, 2015, **6**, 6234.

50 D. Bochicchio and G. M. Pavan, *ACS nano*, 2017, **11**, 1000–1011.

51 D. Bochicchio, M. Salvalaglio and G. M. Pavan, *Nature Communications*, 2017, **8**, 147.

52 A. Gardin, C. Perego, G. Doni and G. M. Pavan, *Communications Chemistry*, 2022, **5**, 82.

53 M. Crippa, A. Cardellini, C. Caruso and G. M. Pavan, *Proceedings of the National Academy of Sciences*, 2023, **120**, e2300565120.

54 P. Gasparotto, D. Bochicchio, M. Ceriotti and G. M. Pavan, *The Journal of Physical Chemistry B*, 2019, **124**, 589–599.

55 J. Chen, M. Wu, L. Gong, J. Zhang, B. Yan, J. Liu, H. Zhang, T. Thundat and H. Zeng, *The Journal of Physical Chemistry C*, 2019, **123**, 4540–4548.

56 H. Lv, Y. Song, H. Zhang, Y. He, X. Hou, J. Sun and X. Wang, *Journal of Molecular Liquids*, 2024, **401**, 124750.

57 T. Wu, Y. Wang, R. Zou, H. Tan, Q. Fu, Y. Liu and M. Ding, *Polymer*, 2024, **303**, 127116.

58 P. Dankers, T. M. Hermans, T. W. Baughman, Y. Kamikawa, R. E. Kieltyka, M. Bastings, H. M. Janssen, N. Sommerdijk, A. Larsen, M. Van Luyn *et al.*, *Advanced materials (Deerfield Beach, Fla.)*, 2012, **24**, 2703–2709.

59 S. I. Hendrikse, S. P. Wijnands, R. P. Lafleur, M. J. Pouderoijen, H. M. Janssen, P. Y. Dankers and E. Meijer, *Chemical Communications*, 2017, **53**, 2279–2282.

60 P. Tiwary and M. Parrinello, *Physical review letters*, 2013, **111**, 230602.

61 C. Caruso, A. Cardellini, M. Crippa, D. Rapetti and G. M. Pavan, *The Journal of Chemical Physics*, 2023, **158**, 214302.

62 C. Caruso, M. Crippa, A. Cardellini, M. Cioni, M. Perrone, M. Delle Piane and G. M. Pavan, *PNAS Nexus*, 2025, **4**, pgaf038.

63 W. P. J. Appel, G. Portale, E. Wisse, P. Y. W. Dankers and E. W. Meijer, *Macromolecules*, 2011, **44**, 6776–6784.

64 A. Barducci, G. Bussi and M. Parrinello, *Physical review letters*, 2008, **100**, 020603.

65 A. Cardellini, M. Crippa, C. Lionello, S. P. Afrose, D. Das and G. M. Pavan, *The Journal of Physical Chemistry B*, 2023, **127**, 2595–2608.

66 M. Crippa, A. Cardellini, M. Cioni, G. Csányi and G. M. Pavan, *Machine Learning: Science and Technology*, 2023, **4**, 045044.

67 M. D. Hanwell, D. E. Curtis, D. C. Lonie, T. Vandermeersch, E. Zurek and G. R. Hutchison, *Journal of cheminformatics*, 2012, **4**, 1–17.

68 M. J. Frisch, G. W. Trucks, H. B. Schlegel, G. E. Scuseria, M. A. Robb, J. R. Cheeseman, G. Scalmani, V. Barone, G. A. Petersson, H. Nakatsuji, X. Li, M. Caricato, A. V. Marenich, J. Bloino, B. G. Janesko, R. Gomperts, B. Mennucci, H. P. Hratchian, J. V. Ortiz, A. F. Izmaylov, J. L. Sonnenberg, D. Williams-Young, F. Ding, F. Lipparini, F. Egidi, J. Goings, B. Peng, A. Petrone, T. Henderson, D. Ranasinghe, V. G. Zakrzewski, J. Gao, N. Rega, G. Zheng, W. Liang, M. Hada, M. Ehara,

View Article Online
DOI: 10.1039/D5TB01272D

K. Toyota, R. Fukuda, J. Hasegawa, M. Ishida, T. Nakajima, Y. Honda, O. Kitao, H. Nakai, T. Vreven, K. Throssell, J. A. Montgomery, Jr., J. E. Peralta, F. Ogliaro, M. J. Bearpark, J. J. Heyd, E. N. Brothers, K. N. Kudin, V. N. Staroverov, T. A. Keith, R. Kobayashi, J. Normand, K. Raghavachari, A. P. Rendell, J. C. Burant, S. S. Iyengar, J. Tomasi, M. Cossi, J. M. Millam, M. Klene, C. Adamo, R. Cammi, J. W. Ochterski, R. L. Martin, K. Morokuma, O. Farkas, J. B. Foresman and D. J. Fox, *Gaussian~16 Revision C.01*, 2016, Gaussian Inc. Wallingford CT.

69 C. I. Bayly, P. Cieplak, W. Cornell and P. A. Kollman, *The Journal of Physical Chemistry*, 1993, **97**, 10269–10280.

70 J. Wang, R. M. Wolf, J. W. Caldwell, P. A. Kollman and D. A. Case, *Journal of computational chemistry*, 2004, **25**, 1157–1174.

71 J. Wang, W. Wang, P. A. Kollman and D. A. Case, *Journal of molecular graphics and modelling*, 2006, **25**, 247–260.

72 M. J. Abraham, T. Murtola, R. Schulz, S. Páll, J. C. Smith, B. Hess and E. Lindahl, *SoftwareX*, 2015, **1**, 19–25.

73 P. Mark and L. Nilsson, *The Journal of Physical Chemistry A*, 2001, **105**, 9954–9960.

74 G. Bussi, D. Donadio and M. Parrinello, *The Journal of chemical physics*, 2007, **126**, 014101.

75 M. Bernetti and G. Bussi, *The Journal of Chemical Physics*, 2020, **153**, 114107.

76 M. Parrinello and A. Rahman, *Journal of Applied physics*, 1981, **52**, 7182–7190.

77 M. Bonomi, D. Branduardi, G. Bussi, C. Camilloni, D. Provasi, P. Raiteri, D. Donadio, F. Marinelli, F. Pietrucci, R. A. Broglia and M. Parrinello, *Computer Physics Communications*, 2009, **180**, 1961–1972.

78 G. A. Tribello, M. Bonomi, D. Branduardi, C. Camilloni and G. Bussi, *Computer Physics Communications*, 2014, **185**, 604–613.

79 D. Reynolds, in *Gaussian Mixture Models*, ed. S. Z. Li and A. Jain, Springer US, Boston, MA, 2009, pp. 659–663.

80 P. Tiwary and M. Parrinello, *The Journal of Physical Chemistry B*, 2015, **119**, 736–742.

81 M. Salvalaglio, P. Tiwary and M. Parrinello, *Journal of chemical theory and computation*, 2014, **10**, 1420–1425.

View Article Online
DOI: 10.1039/D5TB01272D

Data Availability Statement.

The data supporting this article have been included as part of the Supplementary Information (Supporting_Information_UPy-SPs_CPerego.pdf and DATA.zip).
Upon publication the DATA.zip will be published in an open repository.

The authors.